厚生労働科学研究費補助金（免疫アレルギー疾患等予防・治療研究事業）
分担研究報告書

新しい人工足関節の最適化

分担研究者　安達　泰治　京都大学大学院工学研究科機械理工学専攻　准教授

高齢化社会の到来と共に，変形性関節症や関節リウマチといった関節疾患患者への人工関節適応数が増加の一途をたどる中，置換術後の長期安定固定と広い可動範囲に対応した人工関節の開発が，患者の生活の質（QOL）向上のためにも強く望まれている．そこで，我々は，荷重関節の一つである足関節に注目し，生体内の人工足関節および周囲の骨への応力状態を，有限要素法（FEM）を用いた力学解析により検証し，患者の QOL 向上を促す新しい人工足関節の最適設計を試みた．まず，従来の人工足関節の課題を抽出し，これを解決する人工足関節の仕様を検討した．次に，強度試験を並行しながら人工足関節形状の詳細を決定し，人工足関節単体での力学解析を実施した．さらに，足関節近傍に人工足関節が装着された複合モデルを用いた解析を行い，人工足関節周囲の骨の影響について検討した．その結果，骨形態および人工足関節構造を詳細に反映した新しい人工足関節の有意性が確認できた．

1. 研究目的

足関節に重度の破壊をもたらす疾患として，変形性関節症や関節リウマチなどが挙げられる．重篤な疼痛や歩行障害などの機能低下に対して，関節固定術，または，人工足関節置換術の適応となるが，前者においては，関節機能を犠牲にするため，患者の日常生活の質を大きく低下させる．後者においては，関節機能の回復は期待できるが，他の人工股関節や人工膝関節に比べ，術後早期の人工関節の loosening や sinking の発生頻度は少なくない．この原因として，①人工足関節の距腿関節表面における単位面積当りの荷重が過大，②距踵関節が不安定のため術前後の変位が大きい，③インプラント設置の再現性が乏しいため周囲の骨による確実な支持が困難である，が挙げられる．そこで，長期安定性と骨温存が期待できる新たな人工足関節の最適設計を目標とし，特に力学的特性に着目した検討を行った．

従来の人工足関節の課題として，術後早期の人工関節の loosening や sinking の要因である，距腿関節および距踵関節に対する支持性と安定性確保が重要であると考えた．そのため，距腿関節は硬組織である皮質骨の表面に設置する表面置換型距骨コンポーネントを採用し，距踵関節は，距骨と踵骨を連結固定するフィン付距骨ステムを採用した（図 1）．また，距踵関節の固定を必要としない症例も考慮し，距骨コンポーネントと距骨ステムが分離可能なテーパ勘合型モジュラー機構を採用した．さらに，最小限の骨切と柔軟なインプラント設置を考慮し，4コンポーネントによるモバイル構造を採用した．

本研究では，距骨コンポーネントと距骨ステムが力学的に適合しているかを確認するため，まず，簡易形状による強度試験と FEM を用いた力学解析を実施し，人工足関節形状の詳細を決定した．次に，脛骨コンポーネントおよび脛骨ソケットを含んだ人工足関節単体での力学解析を実施し，距骨コンポーネントの剛性並びに応力の集中箇所について検証した．さらに，足関節近傍に人工足関節が装着された複合モデルを用いた解析を行い，人工足関節周囲の骨形態を考慮した時のインプラントおよびインプラント周囲の骨の影響について考察した．

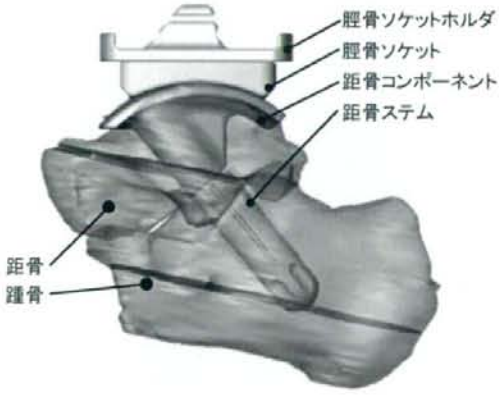

図1．新人工足関節のイメージ図

2. 研究方法

2.1 距骨側インプラントの最適化

図2，3に示すように，距骨ステムの最適形状を模索す

るため，簡易形状による片持ち強度試験を実施した．検討項目は，距骨コンポーネントとの勘合部である距骨ステムのテーパ長さであり，テーパ長さが 6, 8, および 10 mm に対して，テーパ軸方向に 3.5 kN で圧入後，万能力学試験機(EHF-LV010K1-A04，島津製作所製)にて，片持ち強度試験を行い，テーパ勘合強度を計測した．また，テーパ勘合長さの検討に加え，その時の勘合力を後述する片持ち強度試験を再現したFEM解析(図4)の結果と比較することで，力学解析の精度を評価した．次に，同 FEM 解析を用いて，テーパ勘合長さが 8 mm 時の距骨コンポーネントの外径を 9, 10 mm と変化させ，更に外径 9 mm の時のフィンの有無について，それぞれの勘合力を算出し，これらを相対比較することで最適な距骨コンポーネント形状を導いた．

図 2. 距骨コンポーネントおよび距骨ステムの検討項目

図 3. 片持ち強度試験 (3.5 kN 圧入後)

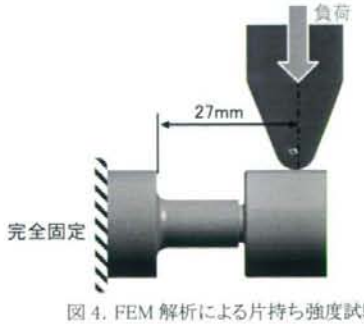

図 4. FEM 解析による片持ち強度試験

2.2 人工足関節単体の FEM 解析方法

図 5 に示すように，前節で決定した距骨コンポーネントおよび距骨ステム形状に加え，脛骨ソケットホルダおよび脛骨ソケットを考慮した人工足関節単体での FEM 解析を行い，人工足関節の応力状態を明らかにした．またその際，距骨コンポーネントの厚みを 2, 2.5, 3 mmと変化させた時の応力状態も検討した．

図 5. 人工足関節単体での FEM 解析モデル

解析手順を以下に示す．まず，3 次元 CAD ソフトウェア(UnigraphicsNX5.0, SIEMENS 社)によりモデリングした人工足関節モデルを汎用 FEM 解析ソフトウェア(MSC.Marc2005, MSC Software 社)へ出力する．次に，1 次の 3 次元 4 面体要素を使用して要素分割を行い，材料物性値，条件設定(荷重条件，拘束条件，接触条件など)を経て解析を行う．人工足関節を構成する Co-Cr-Mo 合金は，ヤング率 239.3 GPa，ポアソン比 0.3，超高分子量ポリエチレン(UHMWPE)は，ヤング率 1.00 GPa，ポアソン比 0.3 を材料定数として設定した(表 1)．荷重条件は，脛骨ソケットホルダより，鉛直下向きに 3,000 N (体重の約 5 倍)負荷し，距骨ステムの遠位端は完全固定した．テーパ勘合部は摩擦係数 0.5 とし，他は摩擦係数 0 とした．

表1. 材料物性値

材質	ヤング率	ポアソン比	降伏応力
Co-Cr-Mo合金	239.3GPa	0.3	1,060MPa
UHMWPE	1.0GPa	0.3	21MPa
皮質骨	17..200MPa	0.3	—
海綿骨	350MPa	0.3	—
セメント(PMMA)	2.643MPa	0.3	67.1MPa

2.3 人工足関節と足関節の複合解析方法

図 6 に示すように，距骨コンポーネントの厚みが 2 mm 時の人工足関節を関節近傍の骨に設置し，脛骨端面から荷重を負荷した時の人工足関節および周囲の骨に発生する応力状態を検証した．解析手順を以下に示す．

人工足関節適応患者の X 線 CT 撮影（京都大学整形外科伊藤宣医師提供）を行い，得られた医用画像（DICOM データ）から，3D 画像処理ソフトウェア Mimics11（Materialise 社）を用いて骨輪郭を抽出し，3D-CAD ソフトウェア Imageware10（SIEMENS 社）を用いて，3D 骨モデルを作成した．次に，3D 骨モデルから各種寸法を計測し，同患者のレントゲン像を参考にしながら最適サイズの人工足関節の 3D モデルをマッチングさせ，臨床に近い状態での人工足関節および骨の複合解析モデルを作成した．足関節周囲の骨形態は，脛骨，距骨，踵骨の 3 種類であり，立位時を想定した．次工程は，前節の解析手順同様，本モデルを FEM 解析ソフトウェアへ出力し，要素分割を行い，材料物性値，条件設定を経て解析を行う．

図 6. 骨に設置した人工足関節の FEM 解析モデル

骨を構成する皮質骨は，ヤング率 17,200 MPa，ポアソン比 0.3，海綿骨は，ヤング率 350 MPa，ポアソン比 0.3，人工足関節を固定するためのセメントは，ヤング率 2,643 MPa，ポアソン比を材料定数として設定した．荷重条件は，脛骨近位端面より脛骨の骨軸に沿って遠位へ 1,500 N 負荷した．拘束条件は，踵骨遠位部の荷重軸方向の変位拘束とし，セメントと人工足関節および骨との接触は完全固着とした．なお，テーパ勘合部は摩擦係数 0.5 とし，他は摩擦係数 0 とした．

3. 結果と考察

3.1 距骨側インプラントの最適化

図 7, 8, 9 に，片持ち強度試験および FEM 解析による荷重－変位曲線と，変位 0.4 mm 時の各条件における von Mises 相当応力分布を示す．図 7, 8 より，テーパ勘合長さが増加すると勘合力は増加傾向にあり，テーパ長さが 8, 10 mm においては，目標値である 3,000 N を満足する勘合力を示した．次に，強度試験と FEM 解析との比較から，変位は異なるものの破断ピーク値はほぼ一致しており，力学解析の精度，すなわち FEM 解析の信頼性が証明された．その他，距骨コンポーネントの外径およびフィンの有無は，図 8, 9 より，同変位における最大応力が低く，かつ負荷に対する変位が少ない外径 9 mm，フィン付（⑤）を採用した．

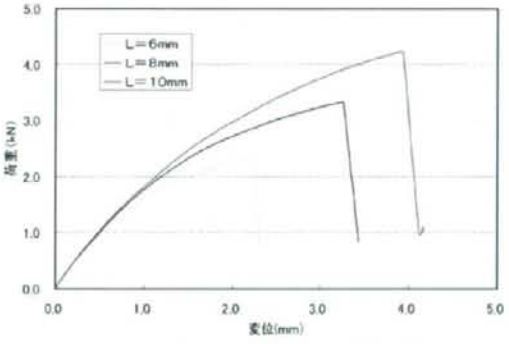

図 7. 強度試験による荷重－変位曲線

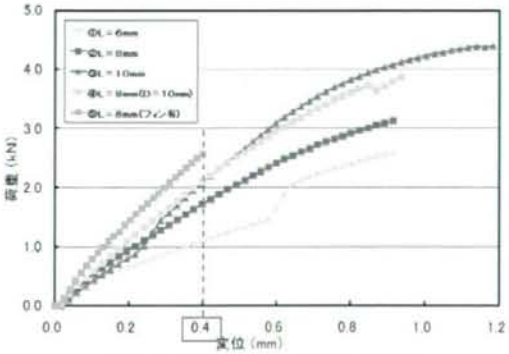

図 8. FEM 解析による荷重－変位曲線

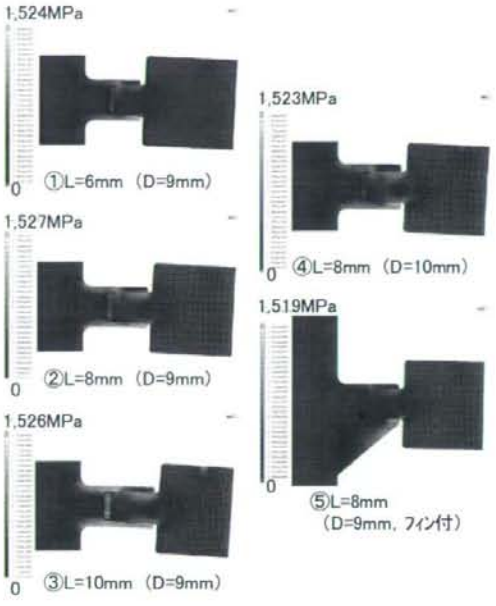

図 9. 各条件における von Mises 相当応力分布（変位 0.4 mm時）

3.2 人工足関節の最適化

図 10 に，距骨コンポーネントの厚みを 2，2.5，3 mmと変化させた時の，人工足関節単体による FEM 解析の von Mises 相当応力分布を示す．図より，距骨コンポーネントの厚みが増加するに従い，距骨側のフィン部から慴動部にかけてのフィレット付近の応力は減少傾向であった．しかしながら，本解析のような過酷な境界条件にもかかわらず，その応力は降伏点の半分以下と低く，距骨コンポーネントの厚みは 2 mm で十分であると判断した．

図 10. 人工足関節を距骨側からみた von Mises 相当応力分布

3.3 人工足関節の骨形態による影響

図 11 に，人工足関節および足関節周囲の骨形態を考慮した von Mises 相当応力分布を示す．上から順に，人工足関節と足関節周囲の骨を組み合わせた応力分布，人工足関節単体の応力分布，足関節周囲の各骨の応力分布を示す．

脛骨端面から負荷した時の人工足関節および周囲の骨に発生する応力は，距腿関節および距踵関節に分布していた．インプラントに着目すると，距骨コンポーネントと距骨ステムの勘合部付近に広い範囲の応力分布が観察された．これは，距骨ステムにより距踵関節を固定したことで，距骨と踵骨の間で生じるせん断力が距骨ステムに働き，結果，勘合部並びにその周辺の応力が高値になったと推測する．また，骨については，踵骨の距骨ステム挿入口付近に高い応力が確認された．これは，インプラントと同様，距骨と踵骨の間で生じるせん断力が，インプラントを通じて距骨に伝達したためと推測する．

図 11. 骨形態を考慮した人工足関節の von Mises 相当応力分布

一方，脛骨遠位および距骨に作用する応力は低く，本研究の目標である足関節周囲の骨によるインプラントの確実な支持性と安定性を示唆する結果となった．また，本解析では，距骨と踵骨のせん断方向への変位拘束は考慮していない過酷な条件にも拘らず，人工足関節および足関節周囲の骨の応力が比較的低い値であった．

以上のことから，実際の足関節に作用する外力負荷とインプラントおよび足関節周囲の骨に働く応力との相互作用については未解明であるが，今回の FEM 解析のように，人工足関節周囲の詳細な骨形態を考慮することは，臨床状態での応力状態を明らかにし，新しい人工関節の開発を行う上で非常に有用であることが示された．

4. 結論

人工足関節の臨床使用における課題を抽出し，これを解決する新しい人工足関節の仕様を検討した．また，力学解析と強度試験を併用し，最適な人工足関節の形状を模索した．臨床使用状態を詳細に反映した足関節近傍の解析モデルを作成し，生体内における人工足関節と骨の応力状態を評価することで，周囲の骨に確実な支持が期待できる人工足関節の設計指標を示した．

以上より，術後の長期安定性と骨温存を兼ね備えた新しい人工足関節の最適設計を確立することができた．

本解析にあたり，ナカシマメディカル(株)野山義裕氏には，多大なるご協力を頂いた．記して謝意を表す．

厚生労働科学研究費補助金（免疫アレルギー疾患等予防・治療研究事業）
分担研究報告書

人工股・膝関節置換術クリティカルパスのアウトカム分析と標準化に向けた検討

研究分担者　宮原寿明　国立病院機構九州医療センター整形外科・リウマチ科　医長

研究要旨　変形性関節症（OA）や関節リウマチ（RA）の股関節破壊に対する人工股関節置換術(THA)は除痛、歩行能力の迅速な改善効果に優れ、早期歩行・社会復帰が可能である。術後療法に対するクリティカルパス（CP）の標準化には、合理的な退院アウトカム設定と、これを裏付ける経過中の部分アウトカム設定も必要である。そこで今回、退院アウトカムに最も影響する自立歩行の達成時期について調査・検討した。また、自立歩行に必要な患肢挙上（straight leg raising: SLR）可能時期、歩行器歩行、1本杖歩行の開始時期、歩行自立（1本杖、）独歩（杖無し歩行）可能時期、歩行自立（1本杖あるいは独歩のいずれか）時期、術後在院日数、CPのバリアンス要因と分類についても評価した。調査対象は2007年11月から2008年10月の1年間に当科で同一術者が手術をおこなったprimary THAの56例63関節手術である。結果：SLR可能時期は術後平均4.0日（1～14日）、歩行器歩行開始時期は平均1.2日（1-4日）、1本杖歩行の開始時期は平均5.4日（4-11日）、歩行自立（1本杖）は平均6.2日（5-10日）、独歩（杖無し歩行）可能例は46/63(73.0%)であり、独歩（杖無し歩行）可能時期は平均10.4日（7-31日）であった。術後在院日数は平均20.2日（14-38日）であった。1週以上退院が遅れた例は3/63例（4.8%）であった。自宅退院は61/63例（96.8%）であり、2/63例（3.2%）が転院した。バリアンス要因は、患者要因（高齢、多関節障害、歩行自立遷延）と社会的要因（家族の受け入れの都合）であった。THAでは、退院のアウトカムとしている1本杖歩行自立が平均6.2日（OA：5.9日、RA：7.3日）で達成されており、2～3週自宅退院の設定はより短縮できる可能性がある。今回、歩行能力と密接に関連するSLR可能時期が術後平均4.0日であったことも歩行自立が早期に可能であることを支持している。早期自立歩行が可能であった理由として、THA手術自体の侵襲の少なさもあるが、術前歩行能力が比較的高い例が多いことも考えられる。今回の調査では、術前歩行自立例が96.8%を占めていた。最近のTHA術後成績では長期耐用性の獲得、術後歩行・運動能力の飛躍的向上が示されており、特に術後早期歩行能力獲得のためには、術前歩行能力が低下する前にTHAをおこなうことが重要と考えられる。今後、術前歩行能力だけでなく、関節破壊度、手術侵襲の程度も加味したTHA-CPのアウトカム決定の試みが必要であると思われる。

A．研究目的

変形性関節症（OA）や関節リウマチ（RA）の股関節破壊に対する人工股関節置換術(THA)は除痛、歩行能力の迅速な改善効果に優れ、早期歩行・社会復帰が可能である。術後療法に対するクリティカルパス（CP）の標準化には、合理的な退院アウトカム設定と、これを裏付ける経過中の部分アウトカム設定も必要である。今回、退院アウトカムに最も影響する自立歩行の達成時期について調査・検討した。

B．方法

調査対象は2007年11月から2008年10月の1年間に当科で同一術者が手術をおこなったprimary THAの56例63関節手術である。疾患別ではOA 44関節、RA 19関節であった。術前の歩行形態・レベルは、歩行自立：61/63(96.8%)、独歩可能（杖無し歩行）：38/63(60.7%)、独歩可能（1本杖歩行）：25/63(39.7%)であった。全例、術前CPDA-1液による全血液状5週保存400mlの自己血貯血を実施。合併症精査の必要の無い症例は基本的に手術前日入院とした。

THAの術後CP:術後1日目から歩行器歩行(全荷重許可)。1～2週で杖歩行。2週以降に正座、胡座、階段昇降練習。2～3週で自宅退院。退院のアウトカム:1本杖あるいは独歩で歩行安定。これらの症例について、患肢挙上（straight leg raising: SLR）可能時期、歩行器歩行、1本杖歩行の開始時期、歩行自立（1本杖、）独歩（杖無し歩行）可能時期、歩行自立（1本杖あるいは独歩のいずれか）時期、術後在院日数、CPのバリアンス要因と分類について評価するとともに、OAとRAで比較検討した。

（倫理面への配慮）

九州医療センター倫理委員会の承認のもとに、インフォームドコンセントを得て各患者の画像および検査データを調査解析した。

C．結果

全体では、SLR可能時期は術後平均4.0日(1～14日)、歩行器歩行開始時期は平均1.2日(1-4日)、1本杖歩行の開始時期は平均5.4日(4-11日)、歩行自立(1本杖)は平均6.2日(5-10日)、独歩(杖無し歩行)可能例は46/63(73.0%)であり、独歩(杖無し歩行)可能時期は平均10.4日(7-31日)であった。術後在院日数は平均20.2日(14-38日)であった。1週以上退院が遅れた例は3/63例(4.8%)であった。自宅退院は61/63例(96.8%)であり、2/63例(3.2%)が転院した。

OAでは、SLR可能時期は術後平均3.5日(1～10日)、歩行器歩行開始時期は平均1.2日(1-4日)、1本杖歩行の開始時期は平均5.2日(4-10日)、歩行自立(1本杖)は平均5.9日(5-9日)、独歩(杖無し歩行)可能例は38/44(86.4%)であり、独歩(杖無し歩行)可能時期は平均10.1日(7-20日)であった。術後在院日数は平均20.4日(14-37日)であった。1週以上退院が遅れた例は2/44例(4.5%)であった。バリアンス要因は、患者要因(高齢、歩行自立遷延)と社会的要因(家族の受け入れの都合)であった。自宅退院は42/44例(96.8%)であり、2/44例(3.1%)が転院した。

RAでは、SLR可能時期は術後平均4.2日(1～14日)、歩行器歩行開始時期は平均1.3日(1-4日)、1本杖歩行の開始時期は平均5.9日(7-11日)、歩行自立(1本杖)は平均7.3日(5-14日)、独歩(杖無し歩行)可能例は8/19(42.1%)であり、独歩(杖無し歩行)可能時期は平均11.0日(7-31日)であった。術後在院日数は平均19.9日(16-35日)であった。1週以上退院が遅れた例は1/19例(5.3%)であった。バリアンス要因は、患者要因(高齢、多関節障害、歩行自立遷延)によるものであった。転院は無かった。

D．考察

THAでは、退院のアウトカムとしている1本杖歩行自立が平均6.2日(OA:5.9日、RA:7.3日)で達成されており、2～3週自宅退院の設定はより短縮できる可能性がある。今回、歩行能力と密接に関連するSLR可能時期が術後平均4.0日であったことも歩行自立が早期に可能であることを支持している。早期自立歩行が可能であった理由として、THA手術自体の侵襲の少なさもあるが、術前歩行能力が比較的高い例が多いことも考えられる。今回の調査では、術前歩行自立例が96.8%を占めていた。最近のTHA術後成績では長期耐用性の獲得、術後歩行・運動能力の飛躍的向上が示されており、特に術後早期歩行能力獲得のためには、術前歩行能力が低下する前にTHAをおこなうことが重要と考えられる。今後、術前歩行能力だけでなく、関節破壊度、手術侵襲の程度も加味したTHA-CPのアウトカム決定の試みが必要であると思われる。

E．結論

THAの術前自立歩行例では、平均1.2日で歩行器歩行開始、平均5.4日で1本杖歩行開始、平均6.2日で1本杖自立歩行、平均10.4日で杖無しでの独歩が可能であった。今後、関節破壊度、手術侵襲の程度、個々の症例のバリアンス予測も加味したCPの部分～退院アウトカム決定の試みが必要であると思われる。

F．健康危険情報

特記すべきことなし

G．研究発表

1．論文発表

1) N Kaibara, H Yamada, T Shuto, Nakashima K, Okazaki H, H Miyahara, Y Esaki, G Hirata & Y Iwamoto:Comparative histopathological analysis between tenosynovitis and joint synovitis in rheumatoid arthritis. Histopathology 2008, 52, 856-864.

2) 熊丸浩仁、宮原寿明、江崎幸雄、平田 剛、糸川高史、橋口智光、桑島海人 CCK(constrained condylar knee)を用いた人工膝関節再置換術の中期成績.日本人工関節学会誌 38:412-413, 2008.

3) 宮原寿明:RA 臼底突出症に対するTHA. Impaction bone graftingを併用したセメントレスカップ設置術.OS NOW instruction.(岩本幸英編集) 9: 48-58, メジカルビュー社, 東京, 2008(分担執筆)

4) 宮原寿明:インフリキシマブによる関節リウマチの荷重関節破壊抑制効果の検討.厚生労働科学研究費補助金免疫アレルギー疾患予防・治療研究事業.平成19年度研究報告書 22-24, 2008.

5) 宮原寿明:人工股・膝関節置換術クリティカルパスのアウトカム分析と標準化に向けた検討.厚生労働科学研究費補助金免疫アレルギー疾患予防・治療研究事業.平成19年度研究報告書 56-59, 2008.

2．学会発表

1) 宮原寿明、江崎幸雄、平田 剛、宮崎 清、糸川高史、今村寿宏、熊丸浩仁、橋口智光:臼蓋cavitary defectに対するimpaction bone grafting併用セメントレスカップ設置の手術手技と中期成績.第38回日本人工関節学会

2008/2/29-3/1 沖縄

2) 熊丸浩仁、宮原寿明、江崎幸雄、平田 剛、糸川高史、橋口智光：関節リウマチ膝に対するCCK(constrained condylar knee)の短・中期成績.第 38 回日本人工関節学会 2008/2/29-3/1 沖縄
3) 今村寿宏、宮原寿明、宮崎 清、江崎幸雄、平田 剛、小原伸夫、橋口智光、糸川高史、熊丸浩仁、桑島海人、安原隆寛、寺田和正：64 例 MDCT を用いた THA 術後 osteolysis の検討.第 38 回日本人工関節学会 2008/2/29-3/1 沖縄
4) 平田 剛、宮原寿明、江崎幸雄、糸川高史、熊丸浩仁、橋口智光：臼蓋 cavitary defect に対する impaction bone grafting 併用セメントレスカップの中期成績.第 52 回日本リウマチ学会総会・学術集会ーワークショップ 2008/4/20-23 札幌
5) 宮原寿明、江崎幸雄、宮崎 清：64 例 MDCT を用いた THA 臼蓋側 osteolysis の検討.第 35 回日本股関節学会 2008/12/5-12/6 大阪
6) 宮原寿明、江崎幸雄、宮崎 清：THA 再置換：GAP shell と impaction bone grafting を用いた臼蓋側高度骨欠損再建の短期成績と bone remodeling の評価.第 35 回日本股関節学会 2008/12/5-12/6 大阪
7) 宮原寿明、江崎幸雄、平田 剛、大石正信、安田廣生、岡田悠子：生物学的製剤使用 RA 手術症例の滑膜炎・関節破壊抑制効果と手術に及ぼす影響の検討.第 36 回日本関節病学会 2008/11/7-11/8 神戸.
8) 宮原寿明、江崎幸雄、平田 剛、大石正信、安田廣生、岡田悠子、近藤正一：RA 手術症例からみた生物学的製剤の滑膜炎・関節破壊抑制効果と手術手技に及ぼす影響.第 23 回日本臨床リウマチ学会 2008/11/29-30 横浜
9) 岡田悠子、宮原寿明、江崎幸雄、平田 剛、大石正信、安田廣生、近藤正一：関節リウマチの人工膝関節 loosening に高度滑膜炎と骨脆弱性の関与が考えられた 1 例.第 23 回日本臨床リウマチ学会 2008/11/29-30 横浜
10) 宮原寿明：生物学的製剤投与 RA 患者に対する手術療法.第 9 回博多リウマチセミナー 2008/1/27 福岡
11) 宮原寿明：DMARDs・生物学的製剤・手術による関節リウマチのタイトコントロール.第 16 回山口県東部地区リウマチ勉強会.2008/5/29 山口
12) 宮原寿明：生物学的製剤・手術による関節リウマチのタイトコントロール.～アクテムラ使用経験を含めて～. アクテムラ適正使用講演会 2008/6/13 熊本
13) 宮原寿明：生物学的製剤・手術による関節リウマチのタイトコントロール.リウマチフォーラム in 岡山 2008/9/20 岡山

H. 知的財産権の出願・登録状況（予定も含む）

1. 特許取得
   なし
2. 実用新案登録
   なし
3. その他
   なし

THA 術後歩行能力回復時期の検討(平均、日)

	SLR 可能	歩行器歩行開始	1 本杖歩行開始	歩行自立(1 本杖)	独歩(杖無し歩行)可能例	独歩(杖無し歩行)
Total (63 例)	4.0 日 (1-14)	1.2 日 (1-4)	5.4 日 (4-11)	6.2 日 (5-14)	46/63 (73.0%)	10.4 日 (7-31)
OA (44 例)	3.5 日 (1-10)	1.2 日 (1-4)	5.2 日 (4-10)	5.9 日 (5-9)	38/44 (86.4%)	10.1 日 (7-20)
RA (19 例)	4.2 日 (1-14)	1.3 日 (1-4)	5.9 日 (7-11)	7.3 日 (5-14)	8/19 (42.1%)	11.0 日 (7-31)

THA 術後退院アウトカムの達成状況

	術後在院日数	1 週以上退院が遅れた例	バリアンス要因	自宅退院	転院
Total (63 例)	20.2 日 (14-38)	3/63 例 (4.8%)	患者要因: 2 例 社会的要因: 1 例	61/63 例 (96.8%)	2/63 例 (3.2%)
OA (44 例)	20.4 日 (14-38)	2/44 例 (4.5%)	患者要因: 高齢、歩行自立遷延 社会的要因: 家族の受け入れの都合	42/44 例 (95.5%)	2/44 例 (4.5%)
RA (19 例)	19.9 日 (16-35)	1/19 例 (5.3%)	患者要因: 高齢、多関節障害、歩行自立遷延	19/19 例 (100%)	0/19 例 (0%)

Ⅲ. 研究成果の刊行物・別刷

J Mater Sci: Mater Med (2008) 19:1009–1016
DOI 10.1007/s10856-007-3076-8

Mechanical, setting, and biological properties of bone cements containing micron-sized titania particles

Koji Goto · Masami Hashimoto · Hiroaki Takadama · Jiro Tamura · Shunsuke Fujibayashi · Keiichi Kawanabe · Tadashi Kokubo · Takashi Nakamura

Received: 18 January 2007 / Accepted: 3 April 2007 / Published online: 1 August 2007

Abstract In this study, polymethylmethacrylate-based composite cements containing 40–55.6 wt% micron-sized titania (titanium oxide) particles were developed, and their mechanical, setting, and biological properties evaluated. Three types of composite cement containing 40, 50, and 55.6 wt% silanized titania were designated ST2-40c, ST2-50c, and ST2-56c, respectively. In animal experiments, ST2-50c and ST2-56c were implanted into rat tibiae and solidified in situ. An affinity index was used to evaluate osteoconductivity. Compressive and bending strength of ST2-56c was 147.7 ± 3.2 and 69.3 ± 7.4; those of the other cements exceeded 100 MPa and 50 MPa, respectively. The affinity indices of ST2-56c were 42.1 ± 12.9 at six weeks and 53.4 ± 16.6 at 12 weeks, and were significantly higher than for ST2-50c and a commercial PMMA bone cement within 12 weeks. Our data indicate that bone cement containing micron-sized titania particles can be applied to prosthesis fixation as well as vertebroplasty, and ST2-56c is a good candidate cement.

K. Goto (✉) · J. Tamura · S. Fujibayashi · K. Kawanabe · T. Nakamura
Department of Orthopaedic Surgery, Faculty of Medicine, Kyoto University, Kawahara-cho 54, Shogoin, Sakyo-ku, Kyoto 606-8507, Japan
e-mail: k.g.bau@kuhp.kyoto-u.ac.jp

M. Hashimoto · H. Takadama
Japan Fine Ceramics Center, Mutsuno 2-4-1, Atsuta-ku, Nagoya 456-8587, Japan

T. Kokubo
Research Institute for Science and Technology, Chubu University, 1200 Matsumoto-cho, Kasugai 487-8501, Japan

Introduction

Since the 1990s, many types of bioactive bone cement have been developed to overcome the disadvantages of polymethylmethacrylate (PMMA) bone cement [1], especially its lack of bone-bonding ability, which occasionally leads to aseptic loosening of prostheses used for arthroplasty [2, 3]. However, the acceptable long-term clinical results of PMMA bone cement [4, 5], and concerns about the long-term stability of bioactive fillers in the cements have so far prevented bioactive bone cements being used for the fixation of prostheses in arthroplasty. Recently, anatase and rutile, crystal phases of titania, have been shown to have excellent in vitro apatite-forming ability and in vivo bioactivity [6–9]. Titania is stable in the body and does not degrade, so that bone cements containing bioactive titania filler can be stable in the body environment. Then a composite bone cement containing nanosized anatase-type titania particles was developed, and it was reported that certain compositions of the cement had good osteoconductivity [10]. However, some of the nanosized titania particles tended to aggregate in the cement. As a result, the cements containing nanosized titania particles did not reach the minimum bending strength required by the ISO 5833 standard (50 MPa), which is applied to acrylic resin cements used for prosthesis fixation, and could be applied clinically for vertebroplasty, but not for prosthesis fixation. One possible resolution of this problem was to increase the titania particle size. In this study, composite cements that contained micron-sized titania particles were developed. Preliminary PMMA cement candidates with different amounts of titania particles were examined for their mechanical properties and apatite forming ability in vitro [11], and two promising composites were used in an implantation study.

The purpose of the study was to evaluate the mechanical and setting properties, and osteoconductivity of cements containing micron-sized titania.

Materials and methods

Preparation of powders

Titania powder

Plate-like titania powder (Ishihara Sangyo Kaisha, Osaka, Japan) with an average particle size of 1.55 μm was used as supplied. The particle size distribution of the titania powder, which was determined using a laser diffraction analyzer (LA-910; Horiba, Kyoto, Japan), is shown in Fig. 1a. Powder X-ray diffraction of the particles revealed that the titania particles were composed of anatase and rutile phases (Fig. 1b). The weight ratio of anatase:rutile in the 1.55 μm titania powder was about one, based on the peak intensities of each diffraction pattern. The titania powder was mixed into three types of TiO_2-dispersed cements with 40, 50, and 55.6 wt% TiO_2, designated ST2-40c, ST2-50c, and ST2-56c, respectively.

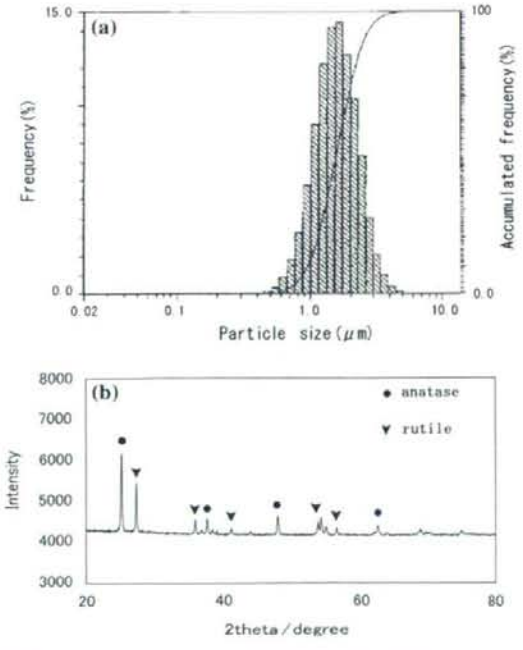

Fig. 1 (**a**) Titania powder particle size distribution. (**b**) Powder X-ray diffraction data for titania powder

Titania powders were treated with a silane-coupling agent as follows: 1.1 g of 3-methacryloxypropyltrimethoxysilane (Shin-Etsu Chemical Co., Tokyo), 1.6 g of ethanol and 0.2 g of deionized water were mixed on a magnetic stirrer for 10 min. The solution containing the silane-coupling agent was added to 110 g of the TiO_2 powder and mixed in a shaker mixer (TURBULA T2F, W. A. Bachofen AG Co., Basel, Switzerland) at 25 °C for 1 h. The rotation speed was 96 rpm. After mixing, the mixtures were dried and heated at 130 °C for 5 min.

Polymethylmethacrylate powder

Spherical PMMA powder, synthesized by suspension polymerization [12], with an average molecular weight of 270,000 Da and an average particle size of 5 μm (standard deviation: 2 μm) [13] was used.

Preparation of the liquid

Liquid methacrylate (MMA) monomer (Wako Pure Chemical Industries, Osaka, Japan) was used.

Cement preparation

Four types of cement, designated ST2-40c, ST2-50c, ST2-56c, and PMMAc, were prepared. PMMAc was a commercially available PMMA-based bone cement (Osteobond; Zimmer, Warsaw, IN, USA) and was used as a control material. The composition of each TiO_2-containing cement is shown in Table 1. As an initiator, benzoyl peroxide (Nacalai Tesque, Kyoto, Japan) was added to the powder at 4.0 wt% of the monomer, and as an accelerator, *N,N*-dimethyl-*p*-toluidine (Kanto Chemical Co. Inc., Tokyo, Japan) was dissolved in the liquid to 2.0 wt% of the monomer. Each cement was prepared by mixing the powder with the liquid for 1 min.

Mechanical testing

The compressive strength, bending strength, and bending modulus of ST2-40c, ST2-50c, and ST2-56c were mea-

Table 1 Composition of PMMA-based cements containing titania powders

Cement	Powders[a] (wt%)		Liquid[b] (wt%) MMA
	Titania	PMMA	
ST2-40c	40	20	40
ST2-50c	50	16.7	33.3
ST2-56c	55.6	14.6	29.6

[a] Benzoyl peroxide was added at 4 wt% of the MMA

[b] *N,N*-Dimethyl-*p*-toluidine was added at 2 wt% of the MMA

sured using five prehardened cement specimens for each mechanical test. For mechanical bending analysis, four-point bending testing was performed with rectangular specimens sized to 70 mm × 20 mm × 5 mm. For compressive mechanical analysis, prehardened cylindrical cement specimens, 6 mm in diameter and 12 mm in length, were prepared. The tests were carried out according to ISO 5833, with a Model 5582 testing machine (Instron Corporation, Canton, MA, USA); the test conditions were previously described in detail [10].

Some of the bending specimens were prepared for observation with a scanning electron microscope (SEM, S-4700; Hitachi, Tokyo, Japan), and the fracture surfaces were analyzed to determine the microstructure of the cements.

Setting of the cements

The cement pastes were mixed for 1 min and cast in a cylindrical mold made of polytetrafluoroethylene (inner diameter 60 mm, inner depth 20 mm). The temperature change during the setting reaction was measured using an infrared thermometer under ambient conditions of 23 °C and 54–65% humidity. By plotting the time and temperature, the setting time of each cement was determined according to ISO 5833.

Animal experiments

Eight-week-old male Wistar rats weighing 180–230 g were used for the implantation study. The animals were reared and the experiments carried out at the Institute of Laboratory Animals, Faculty of Medicine, Kyoto University, under the institutional guidelines for use of experimental animals set by Kyoto University.

The rats were operated on under general anesthesia induced by intraperitoneal injection of sodium 5-ethyl-5-(1-methylbutyl) barbiturate (Nembutal [pentobarbital]; Dainippon Pharmaceutical Company, Osaka, Japan) at 40 mg/kg of body weight. Cortical bone defects measuring 2 mm × 7 mm were created in the medial aspect of the proximal metaphyses of both tibiae, and the bone marrow was curetted. The intramedullary canals of both bone defects were irrigated with physiological saline, and paste-form cement was inserted manually and allowed to cure in situ for evaluation of osteoconductivity [10, 14, 15]. Twelve rats (24 legs) were used for the evaluation of osteoconductivity, with ST2-50c and ST2-56c each being used in 12 legs. Half the rats in each subgroup were killed at six and 12 weeks after the operation.

To confirm the high radiopacity of ST2-56c, another operation was performed using an additional rat. After a hole had been made in the intercondylar space of the distal femur, and the intramedullary canal of the total femur was curetted and irrigated with physiological saline, ST2-56c and PMMAc in liquid phase were inserted into each of the bilateral canals using a syringe fitted with an 18-gauge needle, and this was allowed to cure in situ. One day after the operation, the rat was killed and an X-ray radiograph of the femurs was taken.

Micrographic examination

Specimens were dehydrated through a graded series of ethanol (70, 80, 90, 99, and 100 vol%) and embedded in epoxy resin (Epofix, Struers Co., Copenhagen, Denmark). Thin sections (100 or 500 μm thick) were cut with a band saw (BS-3000; Exakt, Norderstedt, Germany) perpendicular to the axis of the tibias containing the cement. Four sections could be typically made from each leg. The third section (100 μm thick) from the most distal portion of each leg was ground to a thickness of 60–80 μm using a grinding–sliding machine (Microgrinding MG-4000; Exakt) for Giemsa surface staining. The second section (100 μm thick) from each leg was prepared for contact microradiography. The first and fourth sections (500 μm thick) from each leg were polished with diamond paper and coated with a thin layer of carbon for observation by SEM (S-4700, Hitachi, Tokyo, Japan). Some of those specimens were analyzed using an energy-dispersive X-ray microanalyzer (EMAX-7000; Horiba, Kyoto, Japan) attached to the SEM (SEM–EDX). To evaluate osteoconductivity, affinity indices (%) for each subgroup were calculated as previously described [10, 14, 15].

Statistical analysis

Values were expressed as means and standard deviations (SD). Values of mechanical properties for each cement and the affinity indices for each cement at each time interval were compared using one-way analysis of variance. Subsequently, possible differences were investigated using Fisher's PLSD post hoc statistical test using StatView (version 5.0) for Windows. A P value less than 0.01 was considered statistically significant.

Results

Mechanical properties

The results of the mechanical property measurement and their statistical analyses are shown in Table 2. The ultimate compressive strength, flexural strength, and flexural modulus increased as the titania content of the cement increased. SEM revealed that titania particles were

Table 2 Mechanical properties of ST2-40c, ST2-50c, ST2-56c, and PMMAc (means ± SD, $n = 5$)

	Compressive strength (MPa)	Bending strength (MPa)	Bending modulus (GPa)
ST2-40c	106.1 ± 5.5*	54.3 ± 6.6	3.10 ± 0.47
ST2-50c	127.9 ± 6.4*	57.8 ± 4.1	3.88 ± 0.46
ST2-56c	147.7 ± 3.2*	69.3 ± 7.4**	4.07 ± 0.83
PMMAc	87.9 ± 2.7*	59.4 ± 7.8	1.56 ± 0.28***

The values for PMMAc were derived from our previous study[10]

* All pairs were significantly different

** Significantly different to ST2-40c

*** Significantly different to all the other cements

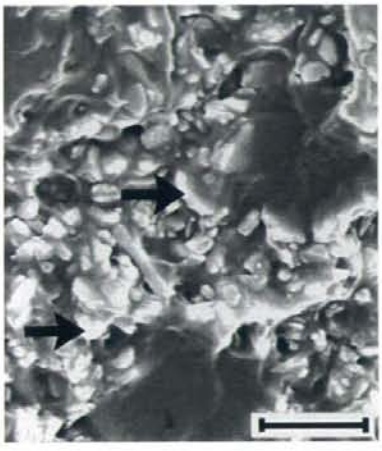

Fig. 2 Scanning electron micrograph of the fracture surface of ST2-56c. Arrows indicate titania particles. Bar = 3 μm

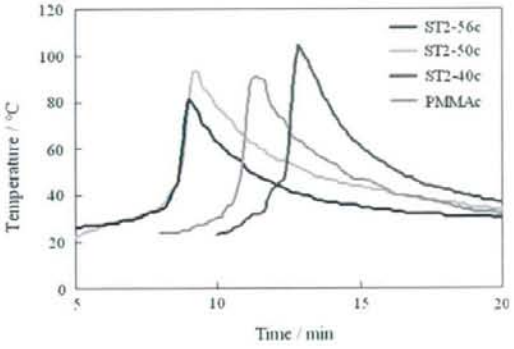

Fig. 3 Heat evolution curves for the setting reactions of ST2-50c, ST2-56c, PMMAc, and ST2-40c

uniformly dispersed and interacted well with the PMMA, and aggregates of titania particles could not be seen in the fracture surfaces of each cement (Fig. 2).

Setting time and peak temperature

The results of the temperature plotting of the cements are shown in Fig. 3. The setting times were 12 min 40 s for ST2-40c, 9 min 0 s for ST2-50c, 8 min 50 s for ST2-56c, and 11 min 0 s for PMMAc. The peak temperatures were 104 °C for ST2-40c, 93 °C for ST2-50c, 81 °C for ST2-56c, and 91 °C for PMMAc. The setting time of the cements containing titania particles reduced and the peak temperature decreased as the titania filler content increased.

Radiopacity

The ST2-56c in the femur was much more radiopaque than the PMMAc (Fig. 4). Both the ST2-56c and PMMAc were injected through an 18-gauge needle without problems, although ST2-56c was more easily injected.

Evaluation of the bone–cement interface

Giemsa surface staining indicated that there was typically no inflammatory reaction around ST2-50c and ST2-56c (Fig. 5a, b). The intervening soft tissue layer between cement and bone was more often seen around ST2-50c than ST2-56c at each time interval. For ST2-56c, no significant change in appearance could be seen with Giemsa surface staining between the 6- and 12-week specimens. On the other hand, for ST2-50c, there appeared to be less intervening soft tissue layer between the cement and bone in the 12-week specimens than in the 6-week specimens.

Low magnification SEM revealed that ST2-56c was in direct contact with bone over large areas within six weeks, whereas ST2-50c was in contact with bone in only small areas (Fig. 6a, b). In the 12-week specimens, both ST2-56c and ST2-50c were in direct contact with bone over large areas (Fig. 6c, d). Both ST2-50c and ST2-56c showed a marginal white line 30–60 μm wide at each time interval,

Fig. 4 X-ray radiograph of bilateral femurs of a rat one day after the operation

regardless of whether they were in contact with bone. These findings were also revealed by contact microradiography, in which each cement appeared to be in direct contact with bone over larger areas than in the SEM observation (Fig. 7a, b).

Backscattered SEM at high magnification revealed that both ST2-56c and ST2-50c were in direct contact with bone within six weeks, but a thin intervening soft tissue layer less than 10 μm thick was often observed between ST2-50c and the bone (Fig. 8a, b). It also showed that ST2-50c and ST2-56c were in contact with bone via a white line, which was demonstrated by SEM–EDX analyses to be a Ti-rich layer (Fig. 8c). An increase in the intensity of calcium was also detected along the outer margin of this white line (Fig. 8c).

Evaluation of osteoconductivity

The affinity indices for all of the cements at six and 12 weeks, and the statistical comparisons, are shown in Fig. 9.

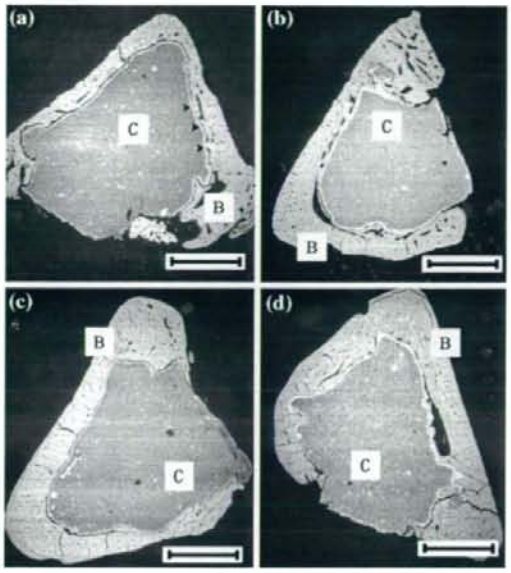

Fig. 6 Low magnification scanning electron micrographs of (**a**) ST2-50c and (**b**) ST2-56c in rat tibiae six weeks after implantation; (**c**) ST2-50c and (**d**) ST2-56c in rat tibiae 12 weeks after implantation. C, cement; B, bone; Arrowheads indicate the white line. Bar = 30 μm

Discussion

In preliminarily trials, it was attempted to prepare cements containing over 60 wt% micron-sized titania particles, but it was often difficult to effectively mix the powder and the liquid. Preliminary in vitro studies revealed that the apatite-forming ability of the composite cements increased with the content of titania particles. Because ST2-50c and ST2-56c were consistently made in a well-mixed form and were expected to have better osteoconductivity than ST2-40c, as judged from the in vitro studies, they were chosen for the animal study.

With the previously reported composite bone cement containing nanosized anatase-type titania particles, it was difficult to disperse the titania particles uniformly in the

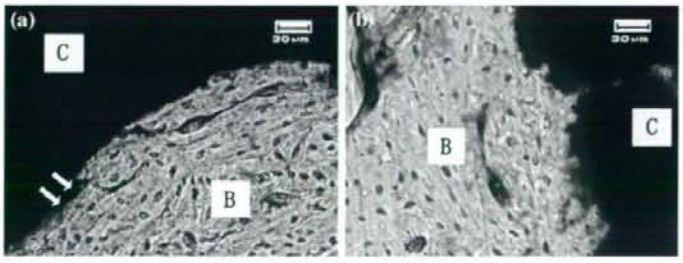

Fig. 5 Giemsa surface staining of (**a**) ST2-50c and (**b**) ST2-56c in rat tibiae 12 weeks after implantation. C, cement; B, bone; Arrows indicate intervening soft tissue. Bar = 30 μm

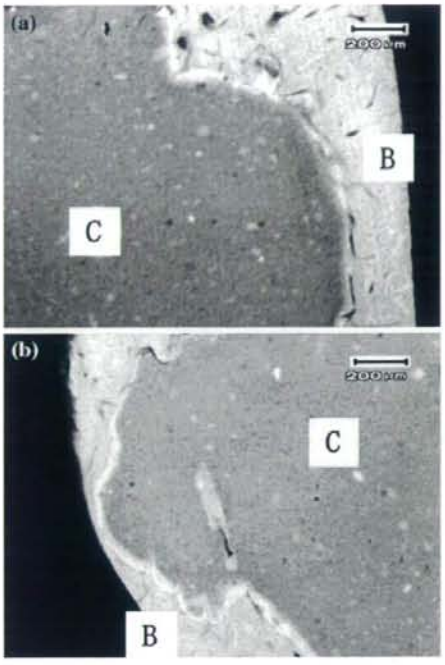

Fig. 7 Contact microradiography of (**a**) ST2-50c and (**b**) ST2-56c in rat tibiae 12 weeks after implantation. C, cement; B, bone. Bar = 200 μm

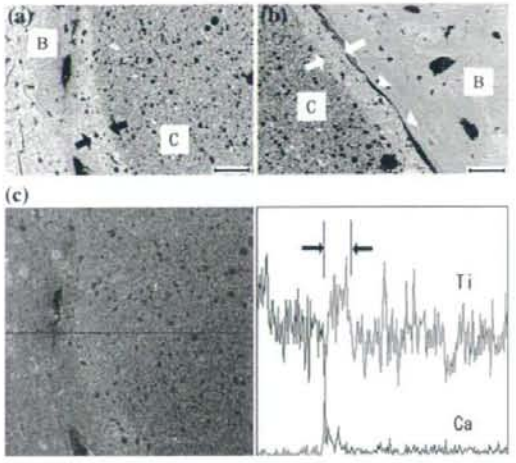

Fig. 8 Back-scattered scanning electron micrographs (SEM) of (**a**) ST2-56c and (**b**) ST2-50c in rat tibiae six weeks after implantation, and (**c**) SEM energy-dispersive X-ray (EDX) analysis of ST2-56c in the same site of (**a**). The white line is clearly visible in (**a**) and (**b**), and SEM–EDX analysis indicated that the white line is a Ti-rich layer. An increase of the intensity of the calcium peak was also detected along the outer margin of the white line. Arrowheads indicate thin intervening soft tissue. Between arrows = white line. C, cement; B, bone. Bar = 40 μm

cement [10]. In contrast, micron-sized particles of mixed-phase anatase–rutile titania dispersed well in the cements, as was shown in this study. Indeed, it is difficult to simply compare the results of the experiments because there was little difference in the experimental conditions including the PMMA/MMA ratio and silanization of the powders. However, the difference in the particle size presumably influenced the degree of the particle dispersion.

The compressive and bending strengths of ST2-50c were much higher than those previously reported for PMMA-based composite cements containing nanosized spherical titania particles at 50 wt%, the compressive and bending strengths of which were 91.8 ± 7.7 and 25.5 ± 9.5 MPa, respectively [10]. Shinzato et al. developed PMMA-based composite cements containing glass beads and reported that a decreasing trend in the bending strength was observed as the glass bead size increased [16]. Their results suggest that cements containing smaller-sized titania could have higher strength. However, our findings were not consistent with theirs, and were presumably influenced mainly by the difference in filler dispersion in our studies, where the micron-sized titania dispersed well, whereas the nanosized titania used in the previous study formed some aggregates in the cement [10]. In this study, there was an increasing trend in

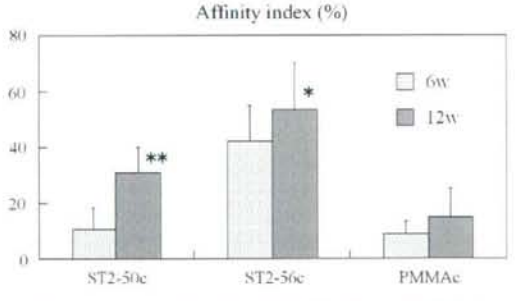

Fig. 9 Affinity indices (%) for ST2-50c, ST2-56c, and PMMAc in rat tibiae at six and 12 weeks after implantation (mean ± SD, $n = 12$). At six weeks, the value for ST2-50c was 10.6 ± 7.8 and 42.1 ± 12.9 for ST2-56c; and at 12 weeks, 30.8 ± 9.0 and 53.4 ± 16.6 respectively. The comparative affinity indices for PMMAc were 8.9 ± 4.4 and 14.9 ± 10.4 at six and 12 weeks, respectively [16]. *Significant compared with ST2-50c and PMMAc at six and 12 weeks. **Significant compared with PMMAc at 12 weeks

compressive strength, bending strength, and bending modulus with increasing titania filler content. Juhasz et al. investigated the effect of filler content on the mechanical properties of AW-glass ceramic–polyethylene composites, and noted that a stiffening effect was observed as the AW-glass ceramic filler content increased from 10 to 50 vol% [17]. Their results were consistent with ours. In this study,

the mechanical strengths of the cements containing micron-sized titania particles met the criteria required by the ISO 5833 standard.

The setting times of the cements containing titania particles in this study were reduced, and the peak temperature decreased, as titania filler content increased. Only ST2-56c exhibited a lower peak temperature than PMMAc, and that of ST2-50c was almost the same as that of PMMAc. This was probably because the weight ratio of PMMA/MMA was 1/2 in ST2-50c, whereas the weight ratio of powder/liquid monomer was about 2/1 in PMMAc, and the content of MMA that polymerizes with an exothermic reaction was almost the same in ST2-50c and PMMAc. As less exothermic setting reactions for bone cement are desirable, both ST2-50c and ST2-56c would be acceptable, but ST2-56c appeared to have lower peak-setting temperature properties and is therefore recommended.

Animal experiments revealed that both ST2-50c and ST2-56c were more osteoconductive than cements containing nanosized titania particles. According to a previous study, the affinity indices of cements containing nanosized titania particles were 20.9 ± 7.3% for cement containing 50 wt% titania particles and 31.3 ± 8.7% for cement containing 60 wt% titania particles at 12 weeks [10]. In the previous study [10] and in this study, high molecular weight PMMA powder was used because it showed low solubility in the MMA monomer during the polymerizing reaction [14]. As a result, bioactive fillers could be exposed at the cement surface without being covered by a layer of polymerized MMA [14]. Therefore, the amount of bioactive particles exposed on the cement surface, which must be proportional to cement bioactivity, was greatly influenced by the particle size of bioactive fillers. In this study, the micron size of the titania particles presumably had a beneficial effect on the osteoconductivity of ST2-50c and ST2-56c. However, ST2-56c was in direct contact with bone over larger areas than ST2-50c, at both six and 12 weeks after implantation into rat tibiae. As well as the larger amount of titania filler, presumably the decrease in toxic monomer content contributed to the higher affinity indices of ST2-56c compared with those of ST2-50c. Further research on bone-bonding strength is necessary to demonstrate the bioactivity of ST2-50c and ST2-56c.

The marginal white line seen on SEM was a Ti-rich layer, as revealed by SEM–EDX analyses (Fig. 8c) and has been similarly observed in cements containing nanosized titania particles [10]. In contrast, it has been reported that PMMA-based composite cement containing glass beads, AW-GC, or hydroxyapatite fillers developed by Shinzato et al. exhibited no such marginal line, although they used a similar PMMA/MMA system and bioactive fillers silanized with γ-methacryloxypropyltrimethoxy silane [14]. Therefore, the properties of the titania filler itself are suggested to contribute to the formation of the white line. Because a Ti-rich layer indicated bioactive titania gathered at the cement surface, it presumably contributes to the osteoconductivity of cements containing titania particles. SEM–EDX analyses also revealed an increase in the concentration of calcium along the outer margin of the white line, which suggests calcium ion transfer or bony tissue invasion into the cement margin. Although a small amount of unpolymerized MMA might leak out of the cement surface, SEM observations revealed no such cement degradation and that leakage was minimal. No toxic effects of the monomer were detected by Giemsa surface staining, and excellent osteointegration of ST2-56c and ST2-50c was seen.

The overall results of this study indicate that PMMA bone cement containing micron-sized titania particles is a promising bone cement for prosthesis fixation as well as for vertebroplasty, but further research on long-term osteointegration and bone-bonding strength should be performed before clinical application.

Conclusions

Three types of PMMA-based composite cements containing 40–56 wt% micron-sized bioactive titania powder were prepared, and their mechanical, setting, and biological properties were evaluated. Compressive strength, bending strength, and bending modulus increased with increasing content of titania filler. The mechanical strengths met the criteria required in the ISO 5833 standard. The peak temperature during the setting reaction decreased as the amount of filler increased, and ST2-56c exhibited a lower peak temperature than commercial PMMA cement. Cements ST2-50c and ST2-56c were revealed to be biocompatible and osteoconductive. This was especially the case with ST2-56c, as it was in direct contact with bone over large areas within six weeks after implantation into rat tibiae, and showed significantly higher affinity indices than those of ST2-50c within 12 weeks. Overall, the data indicate that bone cement containing micron-sized titania particles can be applied to prosthesis fixation as well as vertebroplasty, and ST2-56c is a good candidate cement.

Acknowledgements We greatly appreciate the technical support of Makio Fujioka for the SEM studies.

References

1. S. M. KENNY and M. BUGGY, *J. Mater. Sci. Mater. Med.* **14** (2003) 923
2. M. A. FREEMAN, G. W. BRADLEY and P. A. REVEL, *J. Bone Joint Surg. Br.* **64** (1982) 489

3. S. R. GOLDRING, A. L. SCHILLER, M. ROELKE, C. M. ROURKE, D. A. O'NEIL and W. H. HARRIS, *J. Bone Joint Surg. Am.* **65** (1983) 575
4. F. M. KHAW, L. M. KIRK, R. W. MORRIS and P. J. GREGG, *J. Bone Joint Surg. Br.* **84** (2002) 658
5. J. J. CALLAGHAN, J. E. TEMPLETON, S. S. LIU, D. R. PEDERSEN, D. D. GOETZ, P. M. SULLIVAN and R. C. JOHNSTON, *J. Bone Joint Surg. Am.* **86-A** (2004) 690
6. M. UCHIDA, H. M. KIM, T. KOKUBO, S. FUJIBAYASHI and T. NAKAMURA, *J. Biomed. Mater. Res.* **64A** (2003) 164
7. M. UCHIDA, H. M. KIM, T. KOKUBO, S. FUJIBAYASHI and T. NAKAMURA, *J. Biomed. Mater. Res.* **63** (2002) 522
8. W. Q. YAN, T. NAKAMURA, M. KOBAYASHI, H. M. KIM, J. MIYAJI and T. KOKUBO, *J. Biomed. Mater. Res.* **37** (1997) 267
9. Y. T. SUL, *Biomaterials* **24** (2003) 3893
10. K. GOTO, J. TAMURA, S. SHINZATO, S. FUJIBAYASHI, M. HASHIMOTO, M. KAWASHITA, T. KOKUBO and T. NAKAMURA, *Biomaterials* **26** (2005) 6496
11. T. KOKUBO, S. ITO, Z. T. HUANG, T. HAYASHI, S. SAKKA, T. KITSUGI and T. YAMAMURO, *J. Biomed. Mater. Res.* **24** (1990) 331
12. S. SHINZATO, T. NAKAMURA, T. KOKUBO and Y. KITAMURA, *J. Biomed. Mater. Res.* **54** (2001) 491
13. T. NAKAMURA, H. KATO, Y. OKADA, S. SHINZATO, K. KAWANABE, J. TAMURA and T. KOKUBO, In *Bioceramics*, edited by S. Gianniniand A. Moroni (Bologna: Trans Tech, 2000), p. 661
14. S. SHINZATO, M. KOBAYASHI, W. F. MOUSA, M. KAMIMURA, M. NEO, Y. KITAMURA, T. KOKUBO and T. NAKAMURA, *J. Biomed. Mater. Res.* **51** (2000) 258
15. J. TAMURA, K. KAWANABE, T. YAMAMURO, T. NAKAMURA, T. KOKUBO, S. YOSHIHARA and T. SHIBUYA, *J. Biomed. Mater. Res.* **29** (1995) 551
16. S. SHINZATO, T. NAKAMURA, T. KOKUBO and Y. KITAMURA, *J. Biomed. Mater. Res.* **56** (2001) 452
17. J. A. JUHASZ, S. M. BEST, R. BROOKS, M. KAWASHITA, N. MIYATA, T. KOKUBO, T. NAKAMURA and W. BONFIELD, *Biomaterials* **25** (2004) 949

The Journal of Arthroplasty Vol. 23 No. 5 2008

Contact Stress Analysis of the Conforming Post-Cam Mechanism in Posterior-Stabilized Total Knee Arthroplasty

Yukio Akasaki, MD,* Shuichi Matsuda, MD, PhD,* Takeshi Shimoto, PhD,†
Hiromasa Miura, MD, PhD,* Hidehiko Higaki, PhD,† and Yukihide Iwamoto, MD, PhD*

Abstract: The present study evaluated the effects of extent of conformity of post-cam design on contact area and stress at post-cam mechanism using 4 different posterior-stabilized prostheses. TRAC and Alpina with full-conformed post-cams exhibited the largest contact area at 90° and 120°. PFC sigma RPF with partial conformed post-cam had the largest contact area at 150°. Scorpio NRG with less conformed post-cam had smaller contact area than the others. Lifting of femoral component decreased contact area and increased contact stress of TRAC and Alpina. Recent modifications of post-cam design have increased contact area, contributing to lower contact stress. None of these prostheses exhibited constant low contact stress throughout flexion. Further modifications of post-cam mechanism are necessary to provide lower contact stress throughout deep knee flexion. **Key words:** post-cam, posterior-stabilized, conformity, contact stress, total knee arthroplasty, polyethylene.

Since its introduction in the mid 1970s [1], posterior-stabilized total knee arthroplasty (PS-TKA) has been widely used for patients requiring primary and revision TKA. Long-term follow-up studies have reported satisfactory results [2,3]. The complications of the post-cam mechanism, however, including dislocation of the knee and fracture or severe wear of the post were reported [4-9]. In some retrieval analyses, post damages were found both anteriorly and posteriorly involved in hyperextension and hyperflexion respectively.

*From the *Department of Orthopaedic Surgery, Graduate School of Medical Sciences, Kyushu University, Fukuoka, Japan; and †Department of Mechanical Engineering, Kyushu Sangyo University, Fukuoka, Japan.*
Submitted December 26, 2006; accepted May 18, 2007.
No benefits or funds were received in support of the study.
Reprint requests: Shuichi Matsuda, MD, PhD, Department of Orthopaedic Surgery, Graduate School of Medical Sciences, Kyushu University, 3-1-1 Maidashi, Higashi-ku, Fukuoka, 812-8582, Japan.

0883-5403/08/2305-0015$34.00/0
doi:10.1016/j.arth.2007.05.023

Surgical techniques and rehabilitation programs have been improved to achieve a greater range of movement than 130° to meet the needs of patients who perform deep knee flexions, such as squatting and kneeling, as part of their daily activities [10]. The design of TKA should be modified to achieve the endurance of prosthesis even with deep knee flexion.

A number of biomechanical studies have demonstrated the generation of a high anteroposterior shear force at the tibiofemoral joint during deep knee flexion [11-16]. In our previous study [17], very high contact stress was applied to the post-cam interface, revealing that the shape and apical orientation of the cam affects contact stress significantly. It is reported that high contact stress results in the increasing amount of polyethylene wear in knee wear simulator [18,19]. Therefore, low contact stress is one of the major factors that contribute to prevent polyethylene wear [20-22]. A large contact area and high conformity of the post-cam interface would be necessary to reduce wear problems. Recently, many of post-cam designs have

been modified to contain a larger contact area. It is important to analyze the effects of the conforming post-cam mechanism on the contact stress generated under anteroposterior force with and without lift-off motion, which occurs in deep knee flexion after PS-TKA and causes eccentric loading and premature wear of polyethylene. Many kinematic analyses have demonstrated high and uneven loading applied to the tibiofemoral articular surface with condylar lift-off during knee bending [23-26]. Therefore, primarily, the tibiofemoral articular surface has been modified to reduce edge loading during deep knee flexion. However, the effect of condylar lift-off on contact characteristics of post-cam mechanism should also be evaluated.

This study was designed to evaluate the effects of the extent of the conformity of the post-cam design on the contact area, stress, and location at the post and cam mechanism of PS-TKA, with or without lift-off motion. Four different prosthesis designs were compared. We hypothesized that design characteristics would affect the contact area and stress at each angle of flexion, and lift-off motion alters the loading pattern of each post-cam design. A post-cam interface with a higher degree of conformity could reduce the contact stress of the post-cam mechanism.

Fig. 1. The TRAC prosthesis. This unit has a fully conforming post-cam mechanism.

Materials and Methods

We analyzed the TRAC (Biomet, Warsaw, Ind; size 60 femoral component, size 60 tibial component), the Alpina (Biomet; size 5 femoral component, size 5 tibial component), the PFC sigma RPF (Depuy, Raynham, Mass; size 2 femoral component, size 2 tibial component), and the Scorpio NRG (Stryker, Allendale, NJ; size 7 femoral component, size 5 tibial component) PS-TKAs (Figs. 1-4 respectively). Design feature and size variation are shown in Tables 1 and 2. The experimental method we reported previously [17] was used in the present study. The femoral components were attached to a fixture that provided a flexion range of 90°, 120°, or 150°. The tibial component was implanted into a block of metal in the neutral position. The femoral and tibial fixtures were then mounted into a parallel-link 6-axis actuator.

A compressive posterior load of 500 N was applied to the tibial component against the femoral component parallel to the tibial base plate. The applied load of 500 N was determined according to the biomechanical study of Nagura et al [15]. The position of the femoral component in the sagittal plane was adjusted until both the medial and lateral femoral condyles contacted the tibial articular surfaces. A digital electronic stress sensor (K-Scan sensor, Tekscan Inc, Boston, Mass) was used to detect contact areas and measure contact stresses, placed at the post-cam interface. The sensor has 2 separate sensing areas; each one is 33 × 28 mm and 0.1 mm thick and consists of 26 conductive rows and 22 columns whose intersection points form the sensing location. The device senses the location, timing, and pressure distribution of any contact 0 to 55 MPa with a coating material that varies its electrical resistance with force. An IBM desktop computer connected to the sensor recorded the stress at each intersection. The accuracy of this system has been previously evaluated [27-29]. Measurements were carried out at 90°, 120°, and 150° flexion using the TRAC, Alpina, PFC sigma RPF, and Scorpio NRG components. Measurements were performed 5 times for each component to permit calculation of the variance across the testing conditions. Peak contact stress, defined as the highest stress of all sensing locations, as well as the mean contact stress and contact area were calculated automatically by the Tekscan software. The center of contact area was